The Clay Minerals Society Workshop Lectures Series, Vol. 21 (2016), Chapter 11, 137–149

IMPACT OF MICROSTRUCTURE ON ANION EXCLUSION IN COMPACTED CLAY MEDIA

Christophe Tournassat[1,2]*, Stéphane Gaboreau[1], Jean-Charles Robinet[3], Ian C. Bourg[4], and Carl I. Steefel[2]

[1]*Water, Environment and Ecotechnology Division, French Geological Survey (BRGM), Orléans, 45060, France*
[2]*Earth Sciences Division, Lawrence Berkeley National Laboratory, Berkeley, CA 94720, USA*
[3]*Research and Development Division, ANDRA, Châtenay-Malabry, 92298, France*
[4]*Department of Civil and Environmental Engineering and Princeton Environmental Institute, Princeton University, Princeton, NJ 08544, USA*
e-mail: c.tournassat@brgm.fr

The sensitivity of ion-concentration distribution models to three key model assumptions, the pore-size distribution of clay media, the 'distance of closest approach' of ions to the clay surface, and the accessibility of sub-nanometer-wide clay mineral interlayer spaces to anions, was explored by solving the Poisson-Boltzmann equation for swelling and non-swelling clay materials. The calculations show that all three model assumptions impact significantly on values predicted for the anion-accessible porosity. As a consequence, macroscopic measurements of anion exclusion in clay media cannot be used to test any of the three model assumptions independently of the other two. Information gained at the nanoscale, a detailed characterization of pore-size distribution in particular, is necessary to develop accurate predictive models of the anion accessible porosity of clay media.

1. Introduction

Engineered clay barriers and clay rocks show a remarkable array of macro-scale properties such as high swelling pressure, very low permeability, semi-permeable membrane properties, and a strong coupling between geochemical, mechanical, and osmotic properties (Malusis *et al.*, 2003; Malusis and Shackelford, 2004). In clay media, solute transport is governed primarily by molecular diffusion (Altmann *et al.*, 2012). Experiments have shown repeatedly that anion diffusion in clay media can be described macroscopically by applying a Fickian diffusion model in a fraction of the pore space, the "anion accessible porosity" (Glaus *et al.*, 2010). This finding is consistent with the well known 'anion exclusion' phenomenon, whereby anions are repelled electrostatically from the vicinity of negatively charged clay-mineral surfaces. In contrast, cations are attracted to the clay-mineral surfaces. The general mechanisms associated with anion exclusion and cation adsorption at charged interfaces are well known and are routinely modeled in the framework of theories describing the properties of the 'electrical double layer' (Sposito, 2004; Henderson and Boda, 2009). The exact prediction of the extent of

DOI: 10.1346/CMS-WLS-21.11

anion exclusion in clay materials is, nevertheless, not straightforward. For example, current theories cannot predict precisely the significant difference between anion exclusion in bentonite clay barriers and in clay rocks. In compacted Na-saturated bentonite, anion-accessible porosity is highly sensitive to ionic strength and to the effective dry bulk density of the montmorillonite clay fraction (Van Loon *et al.*, 2007). At low ionic strength and high compaction, the anion-accessible porosity can drop to values that are $<5\%$ of the total porosity value. In highly indurated clay rocks, in contrast, anion-accessible porosity is within a narrow range (30–70% of the total porosity) and exhibits little sensitivity to ionic strength or mineralogy (Descostes *et al.*, 2008; Jacquier *et al.*, 2013). From this simple observation, a consistent model is clearly still not available for quantitative prediction of anion exclusion on the basis of macroscopically measurable properties in different clay materials and as a function of *in situ* conditions. In the following, a description is given about how information gained at the nanoscale through innovative microstructure characterization techniques and modeling methods is required to predict ion distributions in the pore space of nanoporous clay media, and the limits of current models of anion exclusion in clay media are highlighted.

2. Poisson-Boltzmann models of ion distribution in the electrical double layer

2.1. Non-overlapping diffuse layer in 1:1 electrolyte (*e.g.* NaCl)

The electrical double layer (or EDL) can be subdivided conceptually into a 'Stern layer' containing inner- and outer-sphere surface complexes and a 'diffuse layer' containing ions that interact with the surface through long-range electrostatics. The ionic-charge distribution in the EDL is related to the potentials of mean force for the various ions. A simple yet powerful description of this distribution is achieved in the framework of the modified Gouy-Chapman (MGC) model with the underlying assumption that these potentials of mean force are related solely to the local magnitude of the electrostatic potential (Sposito, 2004).

In the MGC model, in the case of an infinite flat surface, ion concentrations in the diffuse layer (c_i) follow a Boltzmann distribution:

$$c_i(y) = c_{i0} \cdot \exp\left(\frac{-z_i \cdot \mathrm{F}\psi(y)}{\mathrm{R} \cdot T}\right) \tag{1}$$

where y is the distance to the edge of the diffuse layer, z_i and c_{i0} are the valence of species i and its concentration in bulk liquid water, respectively, F is the Faraday constant (96,485 C mol^{-1}), R is the ideal gas constant (8.314 J K^{-1} mol^{-1}), and T is absolute temperature (K). The electrostatic potential is calculated from the Poisson equation:

$$\frac{d^2\psi y}{dy^2} = -\frac{1}{\varepsilon}\sum_i z_i \cdot \mathrm{F} \cdot c_i(y) \tag{2}$$

where ε is the dielectric permittivity of water ($78.3 \times 8.85419 \times 10^{-12}$ F m^{-1} at 298 K).

For simple cases, equations 1 and 2 can be solved analytically. For example, in the case of a 1:1 electrolyte such as NaCl in contact with a single surface, the electrostatic potential at a position y is given by:

$$\frac{\mathrm{F}\cdot\psi(y)}{\mathrm{R}\cdot T} = 4\,\mathrm{arctanh}\left[\tanh\left(\frac{\mathrm{F}\cdot\psi_0}{4\cdot\mathrm{R}\cdot T}\right)\times\exp\left(-\kappa\cdot\mathrm{y}\right)\right] \tag{3}$$

where κ is the inverse of the Debye length (κ^{-1} in m):

$$\kappa = \sqrt{\frac{2\cdot\mathrm{F}^2\cdot 1000\cdot I}{\varepsilon\cdot\mathrm{R}\cdot\mathrm{T}}} \tag{4}$$

and ψ_0 is the electrostatic potential at the edge of the diffuse layer:

$$\frac{\mathrm{F}\cdot\psi_0}{\mathrm{R}\cdot T} = -2\cdot\mathrm{arcsinh}\left(\frac{\mathrm{F}^2\cdot|\sigma|}{2\cdot\kappa\cdot\varepsilon\cdot\mathrm{R}\cdot T\cdot\mathrm{N_A}}\right) \tag{5}$$

In equations 4–5, I is the dimensionless ionic strength, $\mathrm{N_A}$ is Avogadro's constant (6.022×10^{23} mol^{-1}), and σ is the surface charge density (C m^{-2}).

By integrating equation 3 an 'anion exclusion distance' can be calculated which corresponds to an equivalent distance from which anions are completely excluded:

$$d_{ex} = \frac{2}{\kappa}\left[1-\exp\left(\frac{\mathrm{F}\cdot|\psi_0|}{2\cdot\mathrm{R}\cdot T}\right)\right] \tag{6}$$

Equation 6 has proved successful at predicting measured anion exclusion distances in very dilute montmorillonite dispersions, thus validating the MGC modeling approach for the case of non-overlapping diffuse layers, *i.e.* the case where the distance between clay particles is sufficiently great that their diffuse layers do not influence each other (Sposito, 1992).

2.2. Compacted clay systems with overlapping diffuse layers in 1:1 electrolyte

In compacted clay systems, the hypothesis of non-overlapping diffuse layers may be invalid, particularly at low salinities or high dry bulk densities. The existence of overlapping diffuse layers can be taken into account by solving equations 1 and 2 numerically for the case of slit-shaped pores between parallel, negatively charged clay surfaces. No means exists, unfortunately, to determine a model-independent value of the electrostatic potential at a surface (Stumm *et al.*, 1976). Direct measurements of ion concentration as a function of distance from a surface also remain extremely arduous, though techniques such as X-ray reflectivity offer some promise in this regard (Bu *et al.*, 2006; Luo *et al.*, 2006). As a consequence, current estimates of the accuracy of the MGC model in compacted clay systems rely primarily on comparisons with the predictions of other models that use more detailed descriptions of the properties

of interfacial liquid water. In the two last decades, molecular-dynamics (MD) simulations have emerged as a powerful technique to unravel the behavior of water and ions in the vicinity of clay-mineral surfaces. Most MD-simulation studies of clay–water interfaces have focused on the structure of the Stern layer (Sposito *et al.*, 1999; Greathouse and Cygan, 2006). The few studies that examined the structure of the diffuse layer (*i.e.* beyond the Stern layer) at clay-mineral surfaces found that the MGC model yielded remarkably accurate predictions, including in systems where diffuse layers overlap, especially if an effective charge for the wall beyond the Stern layer is calibrated on the molecular simulation results (Marry *et al.*, 2002; Tournassat *et al.*, 2009; Bourg and Sposito, 2011; Tinnacher *et al.*, 2016). Those results are in agreement with seminal Monte-Carlo (MC) simulations of the EDL structure, consisting of discrete hard-sphere ions immersed in an implicit solvent, which demonstrate that the MGC model can give accurate results in the case of a 1:1 electrolyte in the vicinity of a charged surface (Carnie and Torrie, 1984).

2.3. Clay systems with multivalent or high-salinity electrolytes

According to MC simulations, the MGC model yields accurate predictions if both anion and cation are monovalent, if c_{i0} does not exceed 0.1 mol dm^{-3}, and if the surface-charge density is not too high (this last condition is fulfilled for clay-mineral surfaces). When divalent (or multivalent) ionic species are present, the MGC model disagrees with MC simulation results under most conditions because it ignores ion-ion correlations in the EDL. For example, for 2:1 electrolytes, the model is inaccurate at salt concentrations of $>$0.005 mol dm^{-3} (Carnie and Torrie, 1984). According to these results, the MGC model should be inaccurate for most, if not all, conditions encountered in natural systems: in low ionic-strength systems, divalent cations (Ca^{2+}, Mg^{2+}) and anions (SO_4^{2-}) represent a non-negligible, if not a major, fraction of adsorbed ions; in high ionic-strength systems, monovalent cations and anions (Na^+, Cl^-) are often the principal species, but the MGC model becomes inaccurate under these conditions in any case. Recent MD simulations, however, suggest that MC simulations with an implicit solvent such as those of Carnie and Torrie (1984) may tend to underestimate the range of conditions over which the MGC model is valid (Tournassat *et al.*, 2014).

3. Microstructural parameters affecting macroscopic ion distribution

3.1. Porosity calculation: where the solid ends and the pore begins

3.1.1. Mean layer density

If the dry bulk density (ρ_{bd}) of a clay medium and the mean clay-mineral layer density (ρ_{layer}) are known, calculation of the porosity (θ) is straightforward:

$$\theta = 1 - \frac{\rho_{bd}}{\rho_{layer}} \tag{7}$$

The mean layer density is an ill-defined parameter, however. The layer density is defined by the ratio of the mass (m_{layer}) and volume of a clay mineral layer (V_{layer}). The latter can be expressed as the product of the surface area of the layer in the *ab* crystallographic plane, $S_{ab,\text{layer}}$, and the thickness of the layer, t:

$$\rho_{\text{layer}} = \frac{m_{\text{layer}}}{V_{\text{layer}}} = \frac{m_{\text{layer}}}{S_{ab,\text{layer}} \cdot t} \tag{8}$$

While the terms m_{layer} and $S_{ab,\text{layer}}$ can be defined rigorously on a crystallographic basis, the term t cannot because the exact boundary between the solid and pore space is not imposed by crystallography alone. Only two values related to the layer thickness can be quantified unambiguously based on crystallography: the distance between the two planes of apical oxygen atoms across a layer, $t_{\text{O-O}}$, and the layer-to-layer distance, t_{int}, *i.e.* the thickness of one layer plus one interlayer space (Figure 1). These two values are not necessarily representative of the thickness of interest, however. Alternatively, the layer density can be measured with volumetric methods, but the measured density is dependent on the distance of closest approach of the probe molecules and, thus, on the effective thickness of the layer probed by

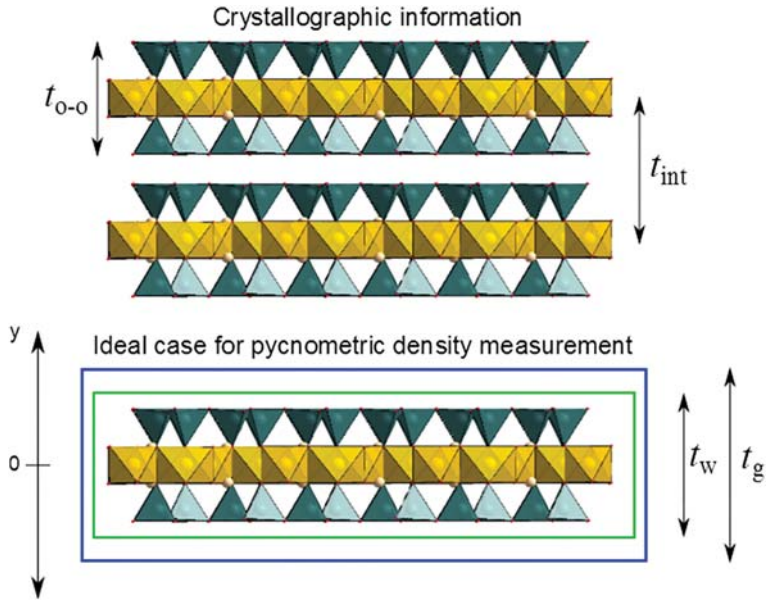

Figure 1. Schematic representation of the various values of layer thickness that can be considered in the calculation or measurement of clay-mineral layer density. The term 'ideal' refers to the fact that only one clay-mineral layer would be probed by the technique. The variables t_{w} and t_{g} refer to the effective layer thickness measured using water or gas molecules.

the technique (t_g in Figure 1). In addition, for swelling clay minerals, volumetric density measurements are carried out under conditions in which clay-mineral layers are stacked. The related density is, thus, representative of a mix of layer thicknesses between t_{int} and t_g.

3.1.2. Effective thickness of hydrated clay layers

The pore space is the volume within which ion-distribution models (such as the MGC model) are applied. It is, thus, convenient to define an effective layer thickness value (t_w) such that the density of pore water equals the density of bulk liquid water ($\sim$1 kg dm^{-3}). Abundant experimental and molecular modeling evidence indicates that water molecules are highly structured within $\sim$1 nm of clay-mineral surfaces, however. The density layering of water near clay surfaces can be described by a density function $\rho_w(y)$, where $y = 0$ refers to the position of the apical oxygen atoms of the clay-mineral layer. If the water-density oscillations extend up to a distance y_1 (or alternatively if y_1 is the location of the pore mid-plane), it is possible to fit a t_w value such that:

$$\frac{1}{y_1 - 1/2 \cdot (t_w - t_{O-O})} \int_{1/2\cdot(t_w - t_{O-O})}^{y_1} \rho_w(y) \cdot dy \approx 1 \text{ kg dm}^{-3} \qquad (9)$$

Application of equation 9 to water-density profiles in MD simulation of pores with a range of pore sizes down to the two-layer (2W) hydrate (Tournassat *et al.*, 2009; Bourg and Sposito, 2011; Hedstrom and Karnland, 2012; Holmboe and Bourg, 2014) yields t_w values of 9.1 $\pm$ 0.3 Å. This value is significantly smaller than the t_{int} value of dry montmorillonite ($\sim$10 Å, depending on the type of interlayer cation). Using available structure parameters (Tournassat and Appelo, 2011), an effective layer density of 2.93 $\pm$ 0.1 kg dm^{-3} can be calculated. This value is greater than the frequently reported montmorillonite pycnometric density of $\sim$2.7 kg dm^{-3}, which corresponds to a layer thickness of 9.9 Å (close to the t_{int} value). For non-swelling clay minerals (such as illite), the thickness value, t_g, should be a good proxy for the 'operational' layer thickness because the layers in the inner part of the particles dominate over the layers located on the outer part of the particles.

3.2. Distance of closest approach and total exclusion volumes

Water molecules can approach the surface more closely than ions located in the diffuse layer. In the MGC model, this effect is taken into account through a 'distance of closest approach' for ions. The accuracy of the MGC model compared to MD results depends on the choice of this distance of closest approach. As a working hypothesis, a distance of 3.5 Å from the apical oxygen atoms can be considered (Tournassat *et al.*, 2009). With this hypothesis, a normalized volume of water corresponding to a thickness of $\sim$1 Å on each surface is considered to be free of ions.

In addition, studies of anion exclusion in clay media sometimes use the simplifying assumption that anions are completely excluded from sub-nanometer-wide clay

interlayer nanopores (Churakov and Gimmi, 2011). The accuracy of this approximation remains unconfirmed. Only two studies have attempted to quantify anion exclusion in the two- and three-layer hydrates of Na-montmorillonite using MD simulations (Rotenberg *et al.*, 2007; Hedstrom and Karnland, 2012). The results of those two studies were contradictory: the former predicted a total Cl^- exclusion from the hydrated interlayer while the latter showed the opposite. Differences in the systems investigated may at least partly explain this discrepancy: Rotenberg *et al.* (2007) studied the two-layer (2W) interlayer hydrate (where the width of the interlayer nanopore equals the thickness of two water monolayers, ~6 Å), while Hedstrom and Karnland (2012) studied a three-layer (3W) hydrate.

3.3. Pore-size distribution

A key measure of pore size is that of the smallest pore dimension, often referred to as the pore width. If the clay mineral is homogeneous and the basal surfaces are perfectly parallel, the mean pore width ($\overline{t_{\text{pore}}}$) can be calculated according to:

$$\overline{t_{\text{pore}}} = \frac{2\theta}{\rho_{\text{bd}} \times SSA_{\text{particle}}} \tag{10}$$

where SSA_{particle} is the specific surface area of the clay-mineral particle, assuming that this surface area is largely dominated by the basal surfaces.

As a first approximation, the anion-accessible porosity of clay media can be predicted by applying the MGC model in a slit-shaped pore of width $\overline{t_{\text{pore}}}$. This simple calculation may underestimate measured values of the anion-accessible porosity, however, because the anion exclusion distance, d_e, is sensitive to pore width in small pores (in conditions where the diffuse layers overlap) but not in larger pores. A closer agreement between experimental results and MGC model predictions can be obtained by assuming that clay media have a non-homogeneous pore-size distribution, which implies that anion-accessible porosity is sensitive to the pore-scale microstructure of clay media (Tournassat and Appelo, 2011; Muurinen *et al.*, 2013).

4. Sensitivity of anion-exclusion predictions to microstructural parameters

4.1. Modeling strategy

In the following, the effects of the various uncertainties identified in the previous section are evaluated in terms of their effect on predictions of the anion-accessible porosity. This analysis is carried out first for compacted montmorillonite samples and then for compacted illite samples.

Mean ion concentrations in the entire pore space, $\bar{C}_i$, were evaluated by discretizing the pore-width distribution into representative domains with discrete pore widths, t_{pore},

with a probability of presence $P(t_{pore})$, calculating the mean concentration $\bar{c}_i(t_{pore})$ in each of these domains, and applying the relation:

$$\bar{C}_i = \frac{1}{\overline{t_{pore}}} \sum_{t_{pore}=0}^{t_{pore\ max}} \bar{c}_i(t_{pore}) \cdot t_{pore} \cdot P(t_{pore}) \quad (11)$$

The relative influence of assumptions regarding the distance of closest approach of ions to the surface, the pore-width distribution, and the extent of anion exclusion from the 2W and 3W interlayer spaces was then investigated on selected examples.

4.2. Ion-concentration distribution in compacted montmorillonite samples

Two dry bulk densities, 1.30 and 1.60 kg dm^{-3}, were chosen as case studies for montmorillonite. A specific surface area of 755 $m^2\ g^{-1}$ (Tournassat and Appelo, 2011) was considered together with a specific surface charge density of −0.11 C m^{-2} which corresponds to a cation exchange capacity of 0.86 $mol_c\ kg^{-1}$. The layer-to-layer distances, t_{int}, for the 3W and 2W interlayer hydrates (at $\rho_{bd,mont} = 1.30$ and 1.60 kg dm^{-3}, respectively) were taken from Holmboe *et al.* (2012) as 19.2 Å and 16.0 Å. The effective layer thickness was taken as 9.1 Å according to the calculations presented in previous sections. The corresponding total water-accessible porosity was $\theta = 0.56$ for $\rho_{bd,mont} = 1.30$ kg dm^{-3} and $\theta = 0.45$ for $\rho_{bd,mont} = 1.60$ kg dm^{-3}. Mean anion concentrations in the pore space were calculated using equation 11 after solving the Poisson-Boltzmann equation numerically for each pore width and for two NaCl bulk concentrations ($[NaCl]_{bulk} = 0.01$ and 0.1 mol dm^{-3}). Five calculation scenarios were considered: (1) the pore size was homogeneous and the ions can access the same volume as water molecules ('hom.1'); (2) the pore size was homogeneous but the ions were excluded from some of the water volume corresponding to a distance of closest approach of 1 Å to the clay surfaces ('hom. clos. app.'); (3) same as 2 but with a bimodal pore-size distribution with 95% of the surface attributed to sub-nanometer-wide interlayer nanopores ('S_{ext} 5%'); (4) same as 3 but with 98% of the surface attributed to the interlayer nanopores (S_{ext} 2%'); and (5) same as 4 but with complete exclusion of anions from the interlayer nanopores ('S_{ext} 2% no int.'). Models 3 and 4 are consistent with X-ray diffraction data that indicate that only a very minor fraction of the surface area does not consist of interlayer nanopores in compacted montmorillonite (Holmboe *et al.*, 2012).

The calculation results are reported in Figure 2 in the form of anion-accessible porosity values ($\theta \cdot \bar{C}_{Cl}/[NaCl]_{bulk}$) together with the range of measured values reported in the literature. Predicted anion-accessible porosities are equally sensitive to model assumptions regarding the distance of closest approach and the accessibility of anions to the interlayer nanopores, but they are most sensitive to the assumed pore-size distribution. Anion-accessible porosity increases significantly as the surface area attributed to interlayer nanopores increases because fewer pores of larger dimension are more favorable to anion accessibility than more pores of smaller dimension. This conclusion echoes the results of Jardat *et al.* (2009) who showed that, depending on the ionic

strength, the anion exclusion can either be dominated by electrostatic effects (at low ionic strength) or excluded volume effects (at high ionic strength). The present calculations also show that the presence or absence of anions in the 2W and 3W interlayer space cannot be determined solely from available macroscopic-scale measurements unless the pore-size distribution is constrained independently.

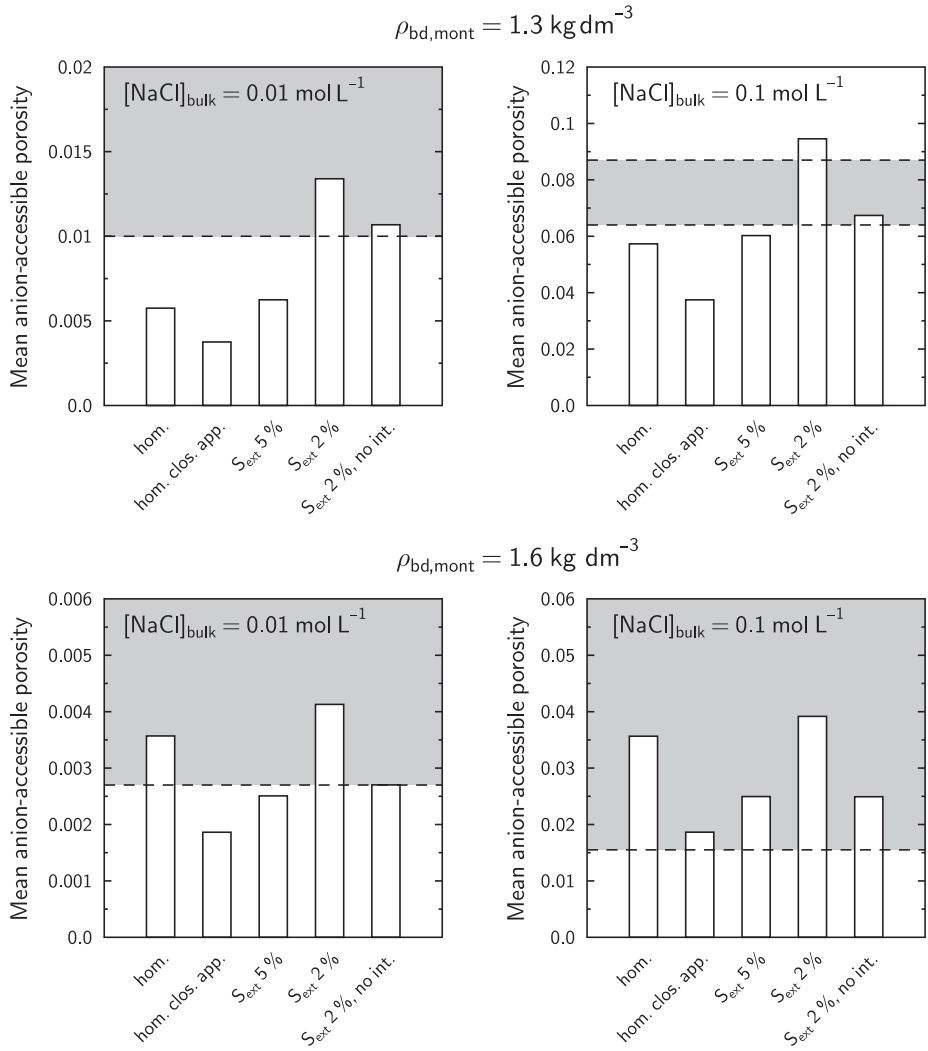

Figure 2. Sensitivity of predicted anion-accessible porosities to three model assumptions: the pore-size distribution of compacted clay; the distance of closest approach of ions to the clay surface; and the accessibility of anions to the clay interlayer nanopores. The gray area corresponds to the range of measured values or to the minimum values reported by Tournassat and Appelo (2011).

4.3. Ion-concentration distribution in compacted illite samples

While the pore-size distribution of compacted montmorillonite cannot be measured currently, recent advances in clay-sample preparation techniques (resin impregnation) and SEM imaging coupled to gas-adsorption techniques can yield accurate data on pore-size distribution in the case of compacted illite, a non-swelling clay mineral (Gaboreau *et al.*, 2016). The resulting pore-size distributions can be used to derive an estimate of the macroscopic-scale anion-accessible porosity. The pore-size distribution obtained for an illite material compacted at $1.7\,\mathrm{kg\,dm^{-3}}$ with $\theta = 0.39$ (Figure 3) was used for anion-accessible porosity predictions. The pore-size

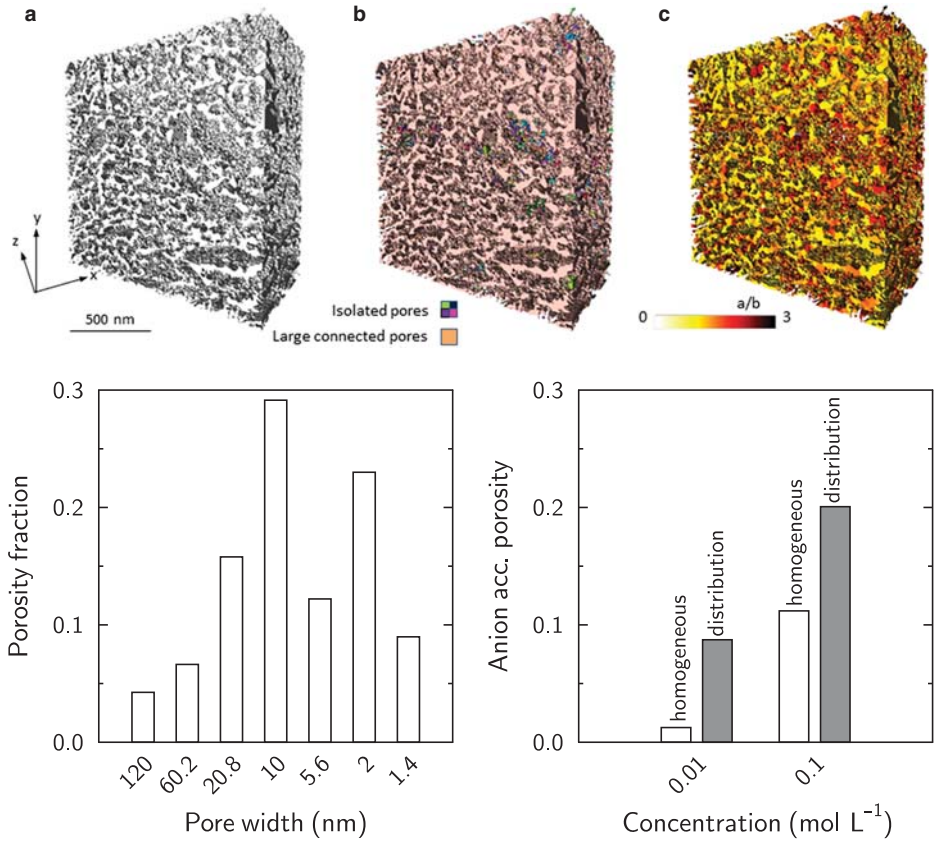

Figure 3. Upper: microstructure of a compacted illite ($1.7\,\mathrm{kg\,dm^{-3}}$, data from Gaboreau *et al.*, 2016). (a) 3-D visualization of a region of interest of 350 × 350 × 180 voxels of the porosity with a voxel resolution size of 5 nm × 5 nm × 5 nm. (b) Components of the segmented pore network. (c) Local shape classification from the computed ellipsoid half-axis length. The color palette indicates the a/b values of the ellipsoid (Brun and Vicente, 2010). Lower left: corresponding pore-width distribution. Lower right: anion-accessible porosity calculation at $[\mathrm{NaCl}]_{\mathrm{bulk}} = 0.01$ and $0.1\,\mathrm{mol\,L^{-1}}$, and assuming an illite layer density of $2.79\,\mathrm{kg\,dm^{-3}}$, a specific surface area of $110\,\mathrm{m^2\,g^{-1}}$, a specific surface charge density of $-0.17\,\mathrm{C\,m^{-2}}$, and either an homogeneous pore-size distribution (white bars) or the measured pore-size distribution gray bars.

distribution was calculated from N_2 adsorption/desorption isotherms and from the analysis (with the assumption of slit-shaped pore geometries) of stacks of images obtained by focused ion beam nanotomography. Mean anion concentrations in the pore space were calculated using equation 11 and the same approach as for the montmorillonite example. As in the case of montmorillonite, anion-accessible porosity is predicted to increase with the heterogeneity of the pore-size distribution (Figure 3): at $I = 0.01$, the anion-accessible porosity accounts for $\sim$3% of the total porosity if pores of homogeneous size are considered, while it accounts for $\sim$22% of the total porosity if the pore-size distribution shown in Figure 3 is taken into account. It is also worth noting that the actual shapes of the pores – from slit-shaped to cylindrical pores – were not considered for this calculation, a factor that could add to the complexity of anion-accessible porosity-data interpretation.

5. Conclusions

A sensitivity analysis based on three key parameters that affect model predictions of anion exclusion in clay media highlighted the significant impact of pore-size distribution on anion-accessible porosity. While recent developments in advanced nano-imaging techniques can provide detailed views of the microstructure of non-swelling materials, determination of the microstructure of swelling clays remains a challenge because important additional information must be obtained at the nanometer to sub-nanometer scale. In addition, the accuracy of ion-distribution models such as the MGC model in sub-nanometer-wide interlayer nanopores is not known for compacted clay systems where EDL overlap is important, particularly with regard to anion accessibility to the interlayer space. Clearly, additional insights from MD simulations (into the structure of the EDL and the accessibility to anions of sub-nanometer-wide interlayer nanopores) are needed to better constrain macroscopic scale models. In natural clay rocks, where both swelling and non-swelling clay minerals are present (smectite, illite, and mixed-layer clay minerals), the characterization of the pore-size distribution (from the micrometer to the nanometer scale) and pore shapes is a necessary step to predict accurately the fraction of the pore space that is accessible to anions. Finally, other sources of uncertainty must also be understood better, including the domain of validity of the MGC model for complex electrolyte compositions or high ionic-strength conditions, the effect of the actual pore geometries, and the fraction of the surface charge that is screened by the Stern layer.

Acknowledgments

The work presented here was supported by the European Atomic Energy Community Seventh Framework Programme [FP7 – Fission – 2009] under grant agreement n°624 249624 Collaborative Project Catclay, from the French ANR SIMISOL project, and by the Director, Office of Science, Office of Basic Energy Sciences,

Chemical Sciences, Geosciences, and Biosciences Division, of the U.S. Department of Energy under Contract No. DE-AC02-05CH11231. C. Tournassat acknowledges funding from L'Institut Carnot for his visit to the Lawrence Berkeley National Laboratory. The image segmentation calculations were carried out using the public-domain software *iMorph* (http://imorph.fr/).

Guest editor: Thorsten Schäfer

The authors and editors are grateful to anonymous reviewers who offered very helpful input and suggestions. A list of all reviewers is given at the end of the Preface for this volume.

References

Altmann, S., Tournassat, C., Goutelard, F., Parneix, J.C., Gimmi, T., and Maes, N. (2012) Diffusion-driven transport in clayrock formations. *Applied Geochemistry*, **27**, 463–478.

Bourg, I.C., and Sposito, G. (2011) Molecular dynamics simulations of the electrical double layer on smectite surfaces contacting concentrated mixed electrolyte (NaCl-$CaCl_2$) solutions. *Journal of Colloid and Interface Science*, **360**, 701–715.

Brun, E. and Vicente, J. (2010) Volumetric segmentation of trabecular bone into rods and plates: a new method based on local shape classification. In: *SPIE Medical Imaging*. International Society for Optics and Photonics, 76234O.

Bu, W., Vaknin, D., and Travesset, A. (2006) How accurate is Poisson-Boltzmann theory for monovalent ions near highly charged interfaces? *Langmuir*, **22**, 5673–5681.

Carnie, S.L. and Torrie, G.M. (1984) The statistical mechanics of the electrical double layer. Pp. 141–253 in: *Advances in Chemical Physics*, **56** (I. Prigogine and S.A. Rice, editors). John Wiley & Sons, Inc., New York.

Churakov, S.V. and Gimmi, T. (2011) Up-scaling of molecular diffusion coefficients in clays: A two-step approach. *The Journal of Physical Chemistry C*, **115**, 6703–6714.

Descostes, M., Blin, V., Bazer-Bachi, F., Meier, P., Grenut, B., Radwan, J., Schlegel, M.L., Buschaert, S., Coelho, D., and Tevissen, E. (2008) Diffusion of anionic species in Callovo-Oxfordian argillites and Oxfordian limestones (Meuse/Haute-Marne, France). *Applied Geochemistry*, **23**, 655–677.

Gaboreau, S., Robinet, J.-C., and Prêt, D. (2016) Optimization of pore network characterization of compacted clay materials by TEM and FIB/SEM imaging. *Microporous and Mesoporous Materials*, **224**, 116–128.

Glaus, M.A., Frick, S., Rosse, R., and Van Loon, L.R. (2010) Comparative study of tracer diffusion of HTO, Na-22(+) and Cl-36(−) in compacted kaolinite, illite and montmorillonite. *Geochimica et Cosmochimica Acta*, **74**, 1999–2010.

Greathouse, J.A. and Cygan, R.T. (2006) Water structure and aqueous uranyl(VI) adsorption equilibria onto external surfaces of beidellite, montmorillonite, and pyrophyllite: Results from molecular simulations. *Environmental Science & Technology*, **40**, 3865–3871.

Hedström, M. and Karnland, O. (2012) Donnan equilibrium in Na-montmorillonite from a molecular dynamics perspective. *Geochimica et Cosmochimica Acta*, 77, 266–274.

Henderson, D. and Boda, D. (2009) Insights from theory and simulation on the electrical double layer. *Physical Chemistry Chemical Physics,* **11**, 3822–3830.

Holmboe, M., Wold, S., and Jonsson, M. (2012) Porosity investigation of compacted bentonite using XRD profile modeling. *Journal of Contaminant Hydrology*, **128**, 19–32.

Holmboe, M. and Bourg, I.C. (2014) Molecular dynamics simulations of water and sodium diffusion in smectite interlayer nanopores as a function of pore size and temperature. *The Journal of Physical Chemistry C*, **118**, 1001–1013.

Jacquier, P., Hainos, D., Robinet, J.-C., Herbette, M., Grenut, B., Bouchet, A., and Ferry, C. (2013) The influence of mineral variability of Callovo-Oxfordian clay rocks on radionuclide transfer properties. *Applied Clay Science*, **83**, 129–136.

Jardat, M., Dufreche, J.F., Marry, V., Rotenberg, B., and Turq, P. (2009) Salt exclusion in charged porous media: a coarse-graining strategy in the case of montmorillonite clays. *Physical Chemical Chemical Physics*, **11**, 2023–2033.

Luo, G., Malkova, S., Yoon, J., Schultz, D.G., Lin, B., Meron, M., Benjamin, I., Vansek, P., and Schlossman, M.L. (2006) Ion distributions near a liquid-liquid interface. *Science*, **311**, 216–218.

Malusis, M.A. and Shackelford, C.D. (2004) Predicting solute flux through a clay membrane barrier. *Journal of Geotechnical and Geoenvironmental Engineering*, **130**, 477–487.

Malusis, M.A., Shackelford, C.D., and Olsen, H.W. (2003) Flow and transport through clay membrane barriers. *Engineering Geology*, **70**, 235–248.

Marry, V., Turq, P., Cartailler, T., and Levesque, D. (2002) Microscopic simulation for structure and dynamics of water and counterions in a monohydrated montmorillonite. *Journal of Chemical Physics*, **117**, 3454–3463.

Muurinen, A., Carlsson, T., and Root, A. (2013) Bentonite pore distribution based on SAXS, chloride exclusion and NMR studies. *Clay Minerals*, **48**, 251–266.

Rotenberg, B., Marry, V., Vuilleumier, R., Malikova, N., Simon, C., and Turq, P. (2007) Water and ions in clays: Unraveling the interlayer/micropore exchange using molecular dynamics. *Geochimica et Cosmochimica Acta*, **71**, 5089–5101.

Sposito, G. (1992) The diffuse-ion swarm near smectite particles suspended in 1:1 electrolyte solutions: modified Gouy-Chapman theory and quasicrystal formation. Pp. 127–156 in: *Clay–Water Interface and its Rheological Implications* (N. Güven and R.M. Pollastro, editors). The Clay Minerals Society, Boulder, Colorado, USA.

Sposito, G. (2004) *The Surface Chemistry of Natural Particles*. Oxford University Press, New York.

Sposito, G., Skipper, N.T., Sutton, R., Park, S., and Soper, A.K. (1999) Surface geochemistry of the clay minerals. *Proceedings of the National Academy of Sciences of the United States of America*, **96**, 3358–3364.

Stumm, W., Hohl, H., and Dalang, F. (1976) Interaction of metal-ions with hydrous oxide surfaces. *Croatica Chemica Acta*, **48**, 491–504.

Tinnacher, R., Holmboe, M., Tournassat, C., Bourg, I.C., and Davis, J. (2016) Ion adsorption and diffusion in smectite clay barriers: molecular, pore, and continuum scale views. *Geochimica et Cosmochimica Acta*, **177**, 130–149.

Tournassat, C. and Appelo, C.A.J. (2011) Modelling approaches for anion-exclusion in compacted Na-bentonite. *Geochimica et Cosmochimica Acta*, 75, 3698–3710.

Tournassat, C., Bourg, I.C., and Steefel, C.I. (2014) Quantification of the breakdown of modified Gouy-Chapman model for 2:1 salt background electrolyte: A molecular dynamic study. In: 248th ACS meeting, San Francisco.

Tournassat, C., Chapron, Y., Leroy, P., and Boulahya, F. (2009) Comparison of molecular dynamics simulations with triple layer and modified Gouy-Chapman models in a 0.1 M NaCl-montmorillonite system. *Journal of Colloid and Interface Science*, **339**, 533–541.

Van Loon, L.R., Glaus, M.A., and Müller, W. (2007) Anion exclusion effects in compacted bentonites: Towards a better understanding of anion diffusion. *Applied Geochemistry*, **22**, 2536–2552.